ACS OMEGA

http://pubs.acs.org/journal/acsodf
Article

Infrared Spectrum and Principal Component Analysis of Heavy Tar Cut by Different Fractions from Tar-Rich Coal

Zhonghua Zhang, Zhao Xue, and Hao Shu*

Cite This: ACS Omega 2024, 9, 1352−1361
Read Online
ACCESS | Metrics & More | Article Recommendations

ABSTRACT: The composition and content of heavy tar vary significantly depending on the pyrolysis conditions and separation methods. This study aimed to effectively identify the main components and content of heavy coal tar and provide a theoretical basis for its subsequent utilization. To achieve this, simulated distillation and infrared spectrum analysis of heavy coal tar were conducted with a focus on understanding the impact of simulated distillation on the composition and structure of tar. The results showed that the fraction content in the tar underwent significant changes after simulated distillation at different temperatures. Specifically, the content of light oil decreased from 4.3 to 0.1%, while the asphalt content increased from 77.6 to 90.6%. Infrared spectrum and peak fitting revealed that the distilled coal tars exhibited similar characteristic peaks in regions associated with hydroxyl, aliphatic hydrocarbon, oxygen-containing functional group, and aromatic hydrocarbon structure. Based on the infrared spectrum of heavy coal tar, principal component analysis was conducted on different fractions. When using two principal components, the cumulative value reached 96.93%. It was found that PC1 displayed strong peak signals around 749 and 687 cm^{-1}, while PC2 exhibited strong peak signals near 2356 and 1143 cm^{-1}.

1. INTRODUCTION

In the current energy landscape, China still heavily relies on coal as its primary energy source and maintains a significant dependence on crude oil and natural gas. The abundance of coal resources in China is a key factor shaping its energy structure based on coal use. However, the conventional combustion of coal not only leads to resources and energy wastage but also contributes to the ecological environment.

In recent years, certain regions in China have discovered coal with a high tar yield designated as tar-rich coal by some scholars. Given its potential for tar and gas resources, it is crucial to explore clean and efficient utilization methods. The byproducts from coal pyrolysis offer valuable applications. Coal tar, in particular, serves as a crucial chemical raw material, with the potential extraction of approximately 10,000 kinds of compounds. In addition, the coal tar can be used to prepare high-value-added chemicals, fuels, and high-quality carbon materials after distillation and separation.

With the increased yield of pyrolysis oil from tar-rich coal, there is a corresponding rise in the production of heavy tar. At present, heavy tar is mainly used to extract chemical substances,[1] synthesize resins,[2] and prepare mesophase pitch.[3] Kalidindi et al.[4] extracted phenol and p-cresol from coal tar. Ozbay and Yargic[5] synthesized porous resin foam, the precursor of foam carbon, using pyrolysis oil. The compressive strength of carbon foam prepared from it is higher than that of conventional phenolic foam. Shi and Ma[6] reviewed the preparation of mesophase pitch by heating and catalytic polycondensation using pitch and tar as raw materials.

While researchers can employ more advanced characteristics methods to differentiate the properties of tar,[7] it is important to acknowledge that some equipment used in the process may destroy the molecular structure of tar. This can have an adverse impact on understanding the chemical structure of its raw materials. Consequently, it is often necessary to combine multiple advanced characterizations to obtain accurate results. In this paper, the heavy coal tar (HCT) fractions were separated by the simulated distillation of gas chromatography, and the characteristics of its components were analyzed. The chemical structure of the tar products cut by different fractions was characterized by FTIR (Fourier transform infrared) spectroscopy, and its structural distribution characteristics were explored. The main wavenumber was analyzed by combining the principal component analysis (PCA) of the infrared spectrum, and the wavenumber range that affected the HCT fractions was obtained. Understanding the composition of HCT has important practical significance for its rational utilization and increasing added value. It can provide a basis for the detection of its structure and performance in the subsequent HCT utilization process.

2. EXPERIMENTAL SECTION

2.1. Experimental Materials. The HCT utilized in this experiment represents the denser fraction obtained during the low-temperature pyrolysis of coal tar. It specifically refers to the submerged heavy tar, which has a density greater than that

Received: October 4, 2023
Revised: December 12, 2023
Accepted: December 18, 2023
Published: December 28, 2023

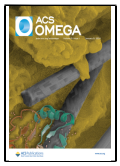

https://doi.org/10.1021/acsomega.3c07671
ACS Omega 2024, 9, 1352−1361

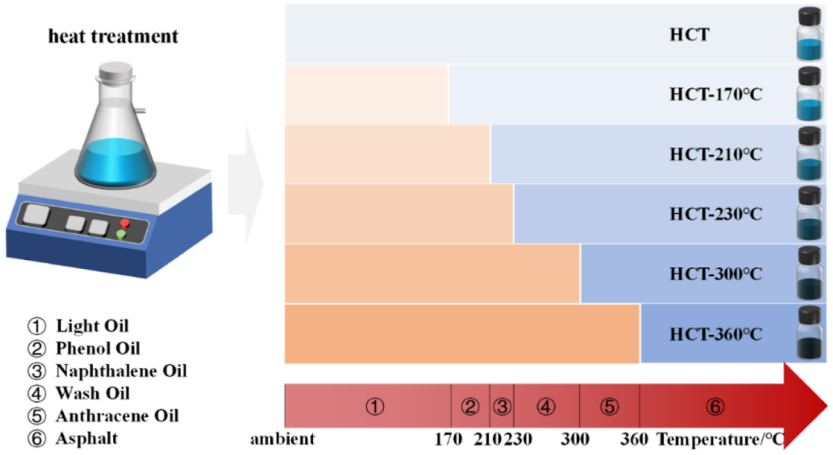

Figure 1. Preparation processes of heavy coal tar cut into different fractions.

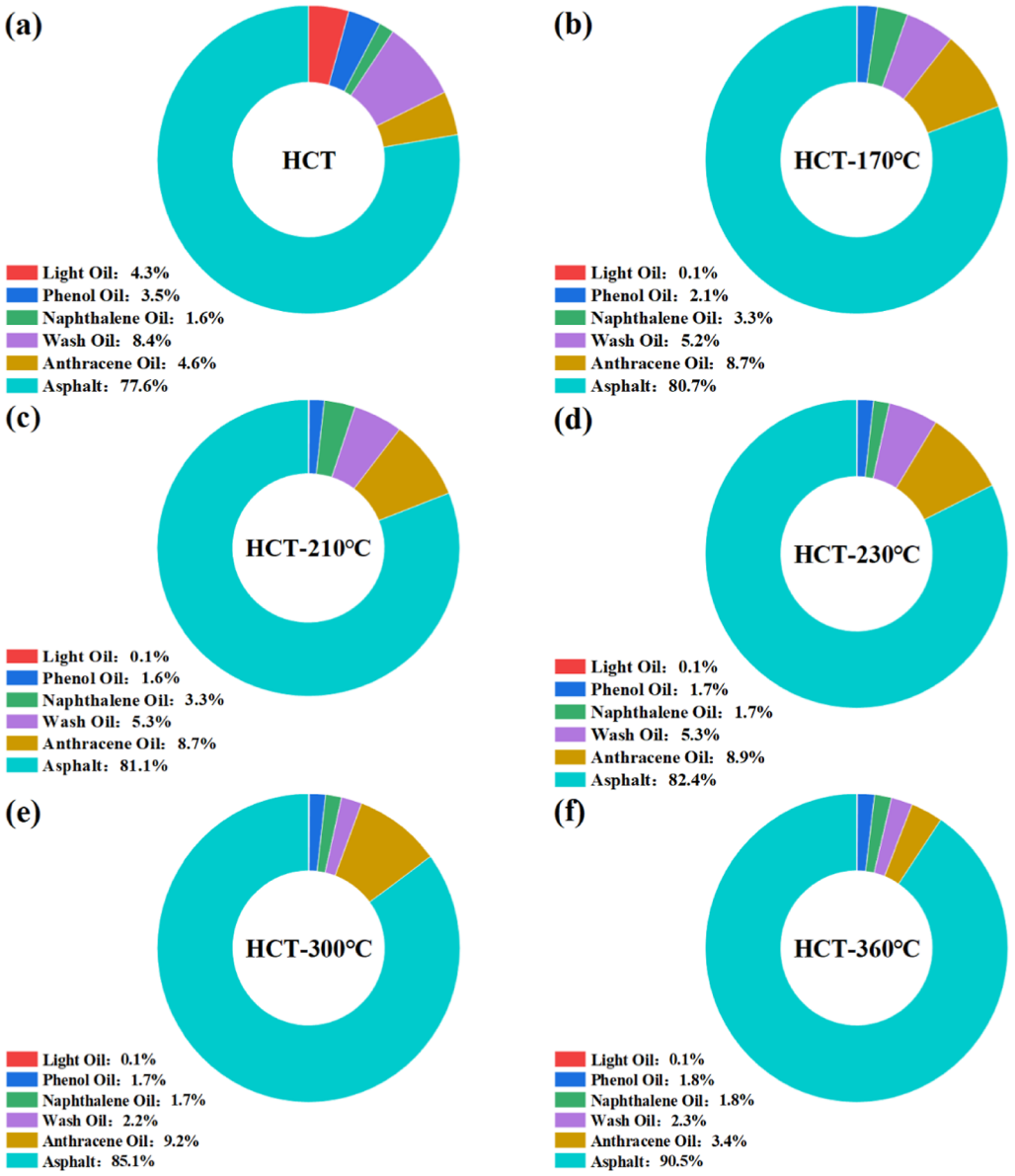

Figure 2. Fraction distributions of heavy coal tar cut by different fractions: (a) HCT, (b) HCT-170 °C, (c) HCT-210 °C, (d) HCT-230 °C, (e) HCT-300 °C, and (f) HCT-360 °C.

https://doi.org/10.1021/acsomega.3c07671
ACS Omega 2024, 9, 1352−1361

of water. Previous research has indicated the existence of tar-rich coal in northern Shaanxi, with high tar production from coal pyrolysis and high production of HCT.[8]

2.2. Experimental Method and Product Analysis. Coal tar is a complex compound with a wide variety of components. Due to the presence of certain components that exhibit convergence at a specific boiling point, distillation is commonly employed for the separation and analysis of coal tar. Distillation temperature is used as a differentiating factor to fractionate coal tar into various components, including light oil (below 170 °C), phenol oil (170−210 °C), naphthalene oil (210−230 °C), wash oil (230−300 °C), anthracene oil (300−360 °C), and asphalt (above 360 °C). In this experiment, HCT was distilled by referring to the treatment methods of different fractions of coal tar and distilled at 170, 210, 230, 300, and 360 °C to obtain coal tar cut by different fractions. As shown in Figure 1, they are named HCT-170 °C, HCT-210 °C, HCT-230 °C, HCT-300 °C, and HCT-360 °C.

The HCT cut by different fractions was simulate distilled, and a GC1100 gas chromatograph was used (Beijing General Analyzer Co., Ltd.) to characterize the composition and content. They were characterized by FTIR spectroscopy with a VERTEX 70 Fourier infrared spectrometer (Bruker Company). The measured spectrum wavenumber range was 4000−400 cm^{-1} with scanning performed 28 times and a resolution of 0.4 cm^{-1}.

3. RESULTS AND DISCUSSION

3.1. Fraction Distribution of Heavy Coal Tar Cut by Different Fractions. Gas chromatography was used to perform a simulated distillation analysis of HCT, and the results are shown in Figure 2. In Figure 2a, HCT is depicted without any pretreatment, with an asphalt content of 77.6% and a small amount of light oil. Figure 2b shows the HCT obtained after distillation at 170 °C, which separates the light oil fraction. As small-molecular organic molecules are either volatilized or decomposed due to the heat, the content of light oil and phenolic oil decreased, while the asphalt increased to 80.6%. Figure 2c shows the HCT obtained after distillation at 210 °C, which separates light oil and phenol oil fractions. The phenolic oil content decreased, and the asphalt increased to 81.0%. Figure 2d shows the HCT obtained by distillation at 230 °C, which separates light oil, phenol oil, and naphthalene oil fractions. With a continuous increase in temperature, the naphthalene oil content decreased and the asphalt content increased to 82.3%. Figure 2e portrays the HCT obtained by distillation at 300 °C, which separates the light oil, phenol oil, naphthalene oil, and wash oil fractions. The content of fraction below the wash oil fraction continued to decrease, while the asphalt content increased to 85.1%. Figure 2f shows the HCT obtained by distillation at 360 °C, which separates other fractions except asphalt. The fraction content below the asphalt decreased, and the asphalt content increased to 90.5%.

3.2. FTIR Analysis of Heavy Coal Tar Cut by Different Fractions. *3.2.1. Distribution of Functional Groups in Heavy Coal Tar Cut by Different Fractions.* The composition of the HCT fractions was observed to vary as the distillation temperature increased. To characterize these different fractions, FTIR was used, and the results were shown in Figure 3. Within the specific number range of 3700−3000 cm^{-1} (hydroxyl structure region), 3000−2800 cm^{-1} (fatty hydrocarbon structure region), 1800−1000 cm^{-1} (oxygen-containing functional group structure region), and 900−600 cm^{-1} (aromatic hydrocarbon structure region),[9] the HCT from different distillation temperatures exhibited relatively similar peaks.[10] This suggests that the components of HCT do not undergo significant changes when it is fractionated at different temperatures. In an effort to gain deeper insight into the difference in the chemical structure between the HCT and HCT fractions obtained at various distillation temperatures, FTIR measurements for the unprocessed HCT were fitted in different structural regions using the Origin software. The semiquantitative analysis was carried out by analyzing the change of functional groups and their respective content in the HCT. The impact of fractionation on the HCT was also assessed by integrating the results from the gas chromatography analysis.

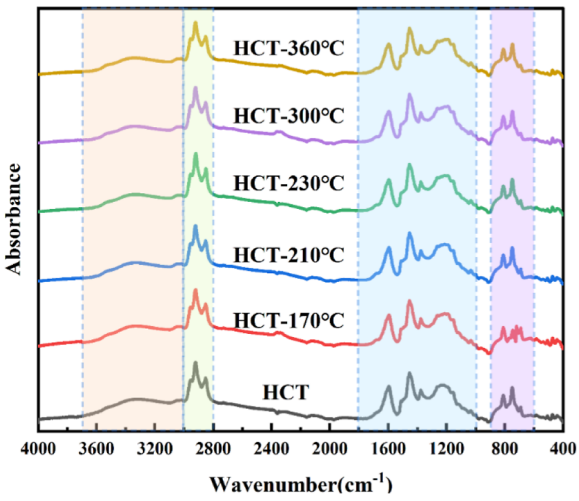

Figure 3. FTIR spectrum of heavy coal tar cut by different fractions.

3.2.1.1. Fitting in the Range of 3700−3000 cm^{-1}. As depicted in Figure 4a−f, the broad absorption peak observed near 3400 cm^{-1} corresponded to the O−H tensile vibration peak, primarily composed of phenolic OH and hydroxyl groups in alkyl.[11] The range of 3100−3000 cm^{-1} represented the vibration peak of aromatic compound −CH.[12] Notably, there was no presence of water molecules −OH between 3700 and 3600 cm^{-1}, which was because the moisture of raw materials disappears after distillation at different temperatures, and only the organic−OH bond was retained.[13] Interestingly, the heavy coal fractions exhibit similar peak positions and peak values across different fractions. This indicates that the chemical structure of the fractions in the hydroxyl structure region remains largely unaffected.

3.2.1.2. Fitting in the Range of 3000−2800 cm^{-1}. The spectrum of all samples had strong bands between 3000 and 2800 cm^{-1}[14], as shown in Figure 5a−f. At 2920 and 2850 cm^{-1}, the stretching vibration peak of aliphatic C−H and the antisymmetric stretching vibration peak of saturated C−H on methyl ($-CH_3$) were respectively,[15] and the stability of the peak indicated that the aliphatic content had not increased.[16]

3.2.1.3. Fitting in the Range of 1800−1000 cm^{-1}. As shown in Figure 6a−f, the concentration range of the C−O group was from 1800 to 1000 cm^{-1}, encompassing the C−O tensile vibration peak at approximately 1705−1650 cm^{-1}, the C−O−C vibration peak at 1280 cm^{-1}, and the C−O vibration peak at 1090 cm^{-1}.[17] The range of 1620−1500 cm^{-1} represents the C═C tensile vibration peak.[18] Around 1600 cm^{-1}, the most common aromatic hydrocarbon functional

https://doi.org/10.1021/acsomega.3c07671
ACS Omega 2024, 9, 1352−1361

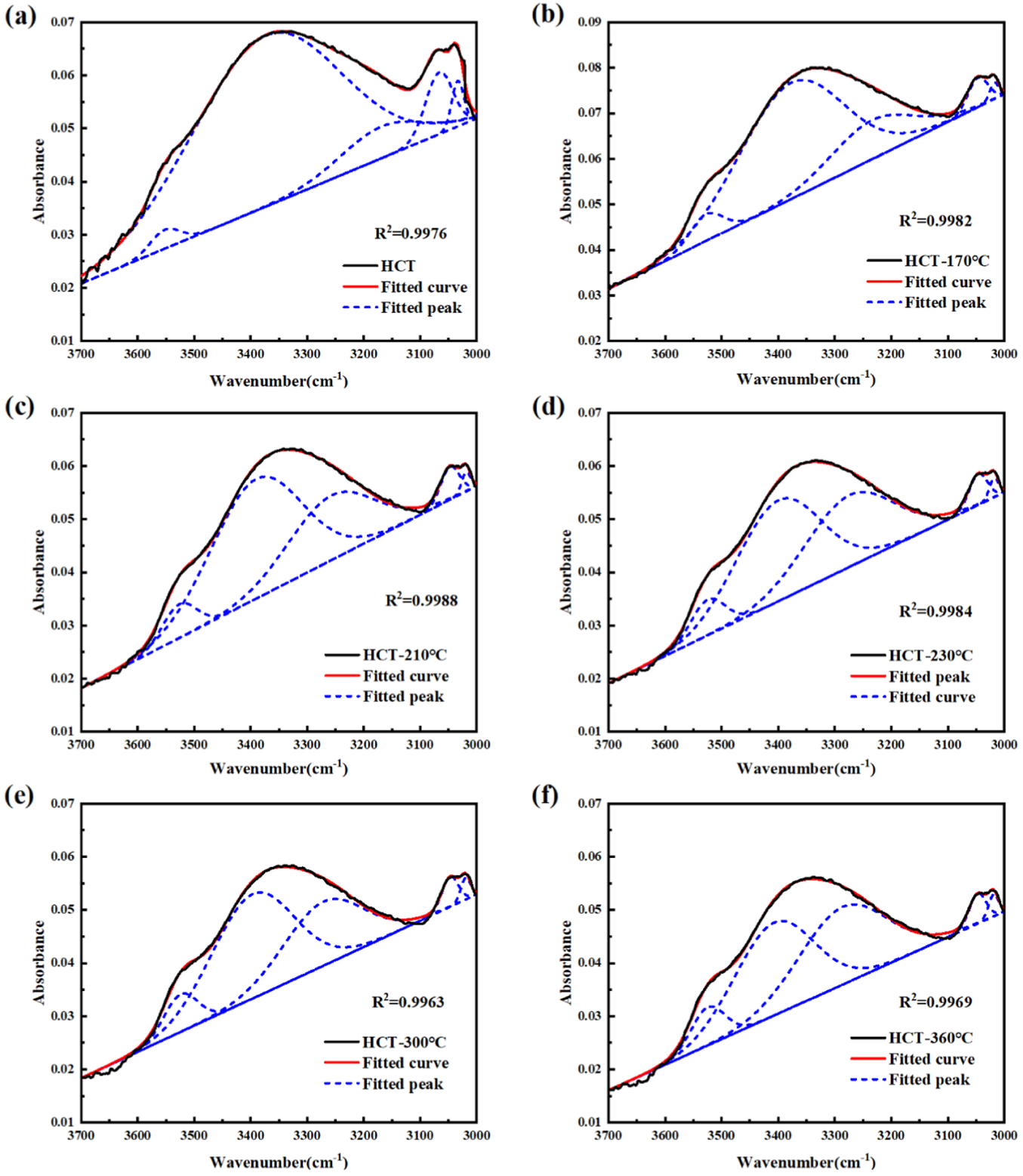

Figure 4. Fitting curve in the range of 3700−3000 cm^{-1}: (a) HCT, (b) HCT-170 °C, (c) HCT-210 °C, (d) HCT-230 °C, (e) HCT-300 °C, and (f) HCT-360 °C.

group in HCT is observed, with sharp and strong peaks varying among HCT fractions. The higher the aromatic hydrocarbon content, the greater the condensation degree. Despite changes in the distillation temperature, the peak value remains relatively stable, suggesting insignificant alterations in the condensation degree among different HCT fractions. The −CH bending vibration peaks are evident at around 1450 and 1380 cm^{-1}.[19] A prominent absorption peak between 1300 and 1000 cm^{-1}, constituting over one-third of the fitting peak, is attributed to the C−O stretching vibration peak of alkyl ether. The ether bond serves as the primary bridge bond in the aromatic structure of coal and tar molecule. However, as the

https://doi.org/10.1021/acsomega.3c07671
ACS Omega 2024, 9, 1352−1361

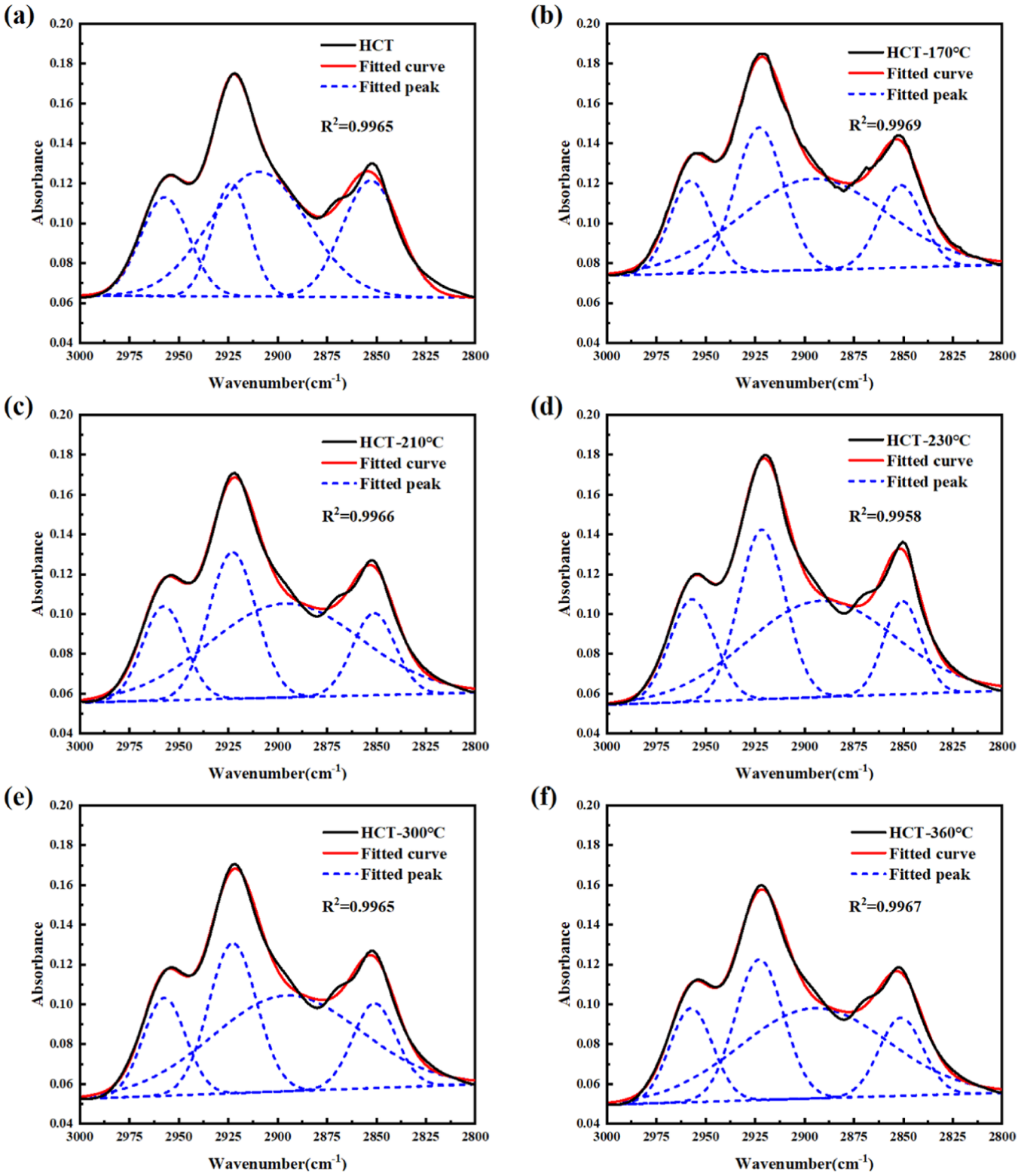

Figure 5. Fitting curve in the range of 3000−2800 cm^{-1}: (a) HCT, (b) HCT-170 °C, (c) HCT-210 °C, (d) HCT-230 °C, (e) HCT-300 °C, and (f) HCT-360 °C.

temperature surpasses 300 °C, a decline in peak value indicates the temperature's impact on the existence of ether bonds. The peak values between 1500 and 1350 cm^{-1} signify the presence of methyl in HCT. Moreover, with the increase in distillation temperature, the intensity of the fitting peak of the curve between 1200 and 1000 cm^{-1} gradually intensifies.

3.2.1.4. Fitting in the Range of 900−600 cm^{-1}. According to the fitting curve in Figure 7a−f, there are multiple peaks in the range of 900−600 cm^{-1},[20] primarily corresponding to the vibrational modes of aromatic C−H bonds, which involve the out-of-plane bending of these bonds.[10] This suggests that aromatic rings contain numerous substituents.[21] Specific to the

https://doi.org/10.1021/acsomega.3c07671
ACS Omega 2024, 9, 1352−1361

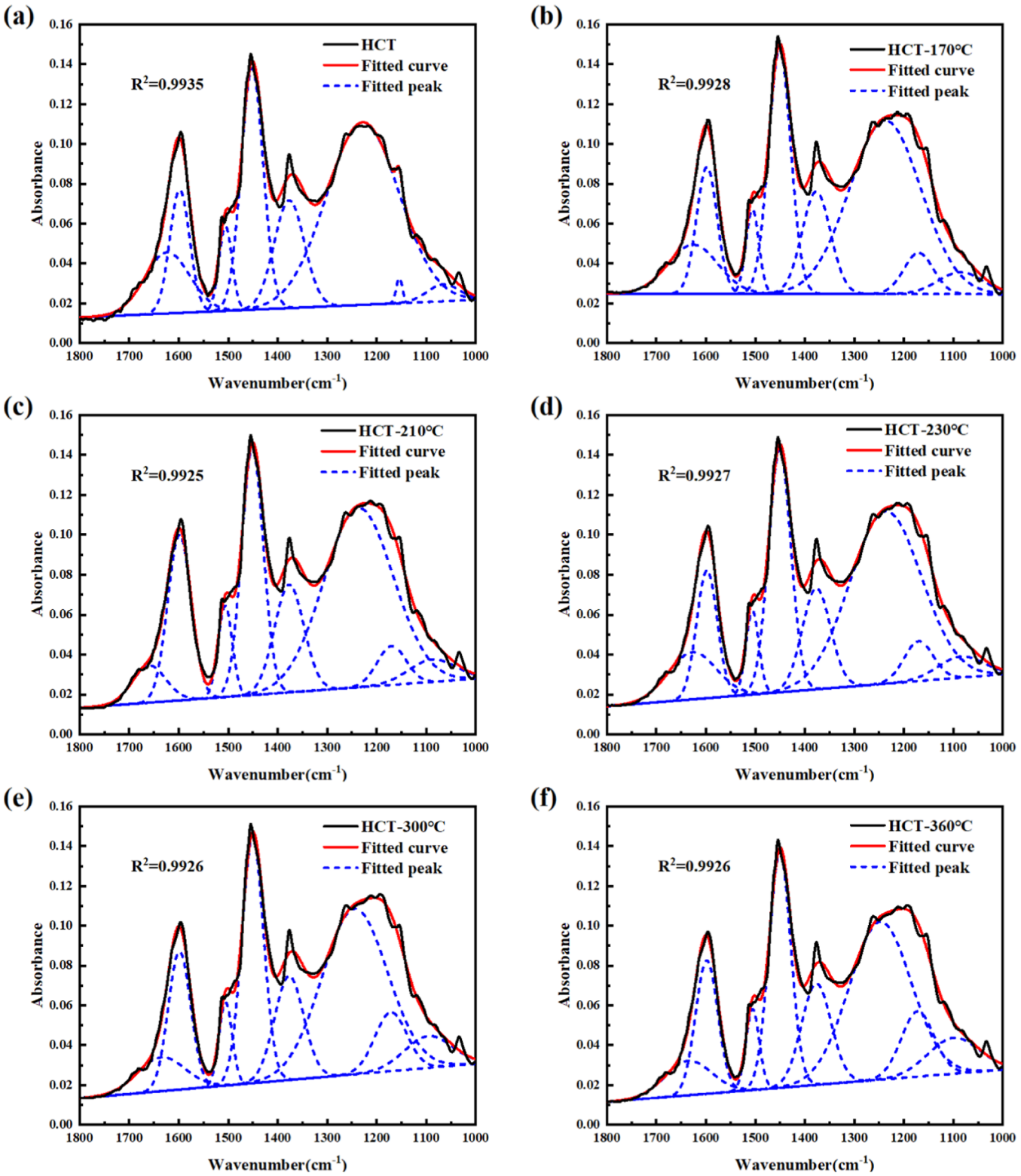

Figure 6. Fitting curve in the range of 1800−1000 cm^{-1}: (a) HCT, (b) HCT-170 °C, (c) HCT-210 °C, (d) HCT-230 °C, (e) HCT-300 °C, and (f) HCT-360 °C.

aromatic substituted hydrocarbons, CH (adjacent H, adjacent 2H, and adjacent 4H) exhibits characteristic peaks at 875, 810, and 750 cm^{-1}, respectively.[22] However, these peaks have relatively weak intensities, and the intensity of their vibrational peak decreases as the distillation temperature rises. This phenomenon implies that the increased distillation temperature leads to a bridge bond within the functional group of aromatic hydrocarbons. Furthermore, it is worth noting that the R^2 values for each fitting peak are consistently higher than 0.99, indicating a strong conformity between the fitting and the infrared spectrum (peak 23). This high level of agreement underscores the reliability of the fitting analysis.[23]

https://doi.org/10.1021/acsomega.3c07671
ACS Omega 2024, 9, 1352−1361

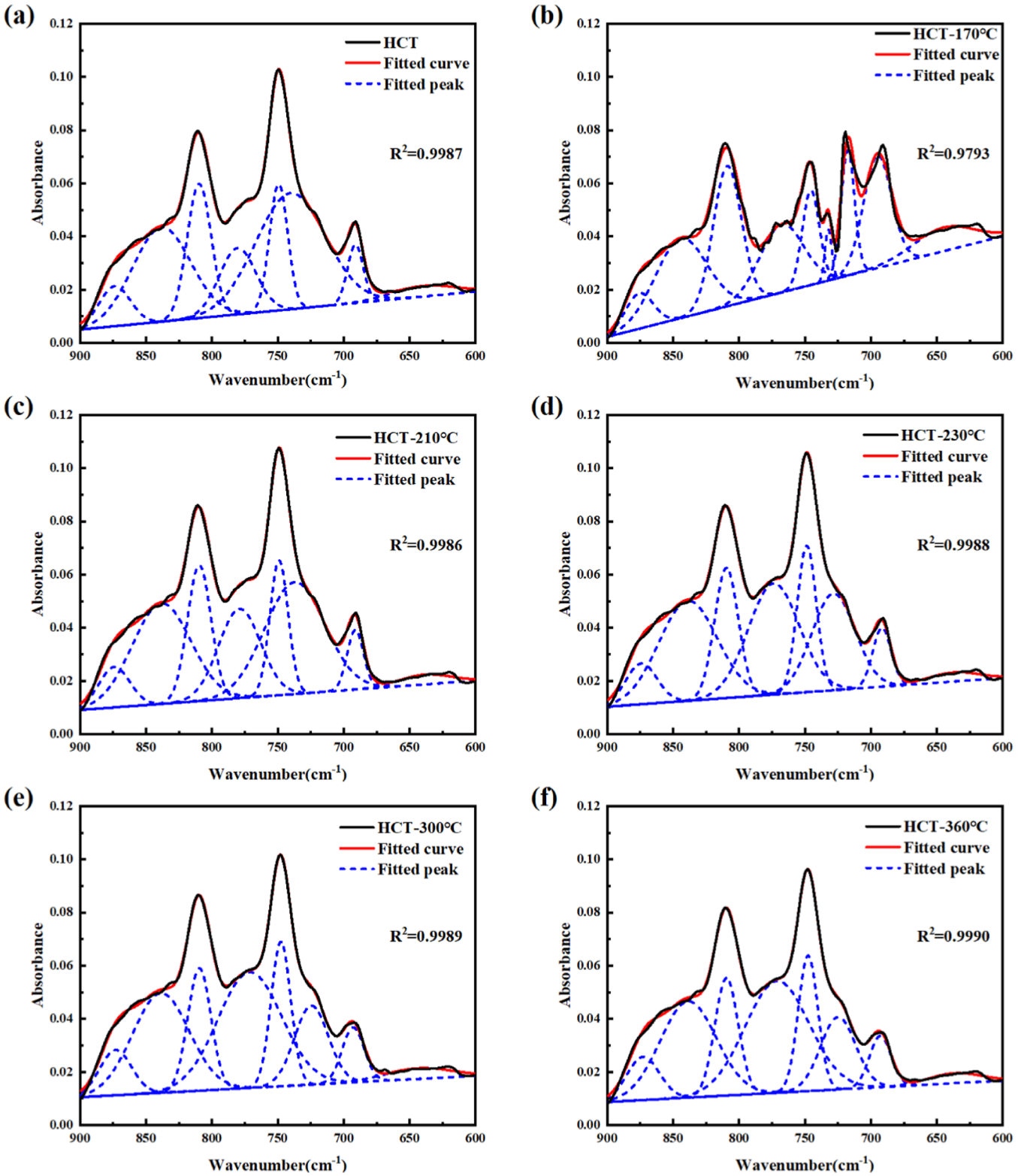

Figure 7. Fitting curve in the range of 900−600 cm^{-1}. (a) HCT, (b) HCT-170 °C, (c) HCT-210 °C, (d) HCT-230 °C, (e) HCT-300 °C, and (f) HCT-360 °C.

3.3. Principal Component Analysis of HCT Cut by Different Fractions. In the regions depicted in Figure 8a−c, the distribution of fitting peaks of different fractions of HCT in the hydroxyl structure region, fatty hydrocarbon structure region, and oxygen-containing functional group structure region appeared to be relatively concentrated. This suggests that the fitted curves closely aligned with the actual data in these specific regions, while the distribution in the aromatic hydrocarbon structure region, as shown in Figure 8d, appeared more dispersed, reflecting the complexity and diversity of functional groups in the sample, which was caused by different products in the raw materials.

https://doi.org/10.1021/acsomega.3c07671
ACS Omega 2024, 9, 1352−1361

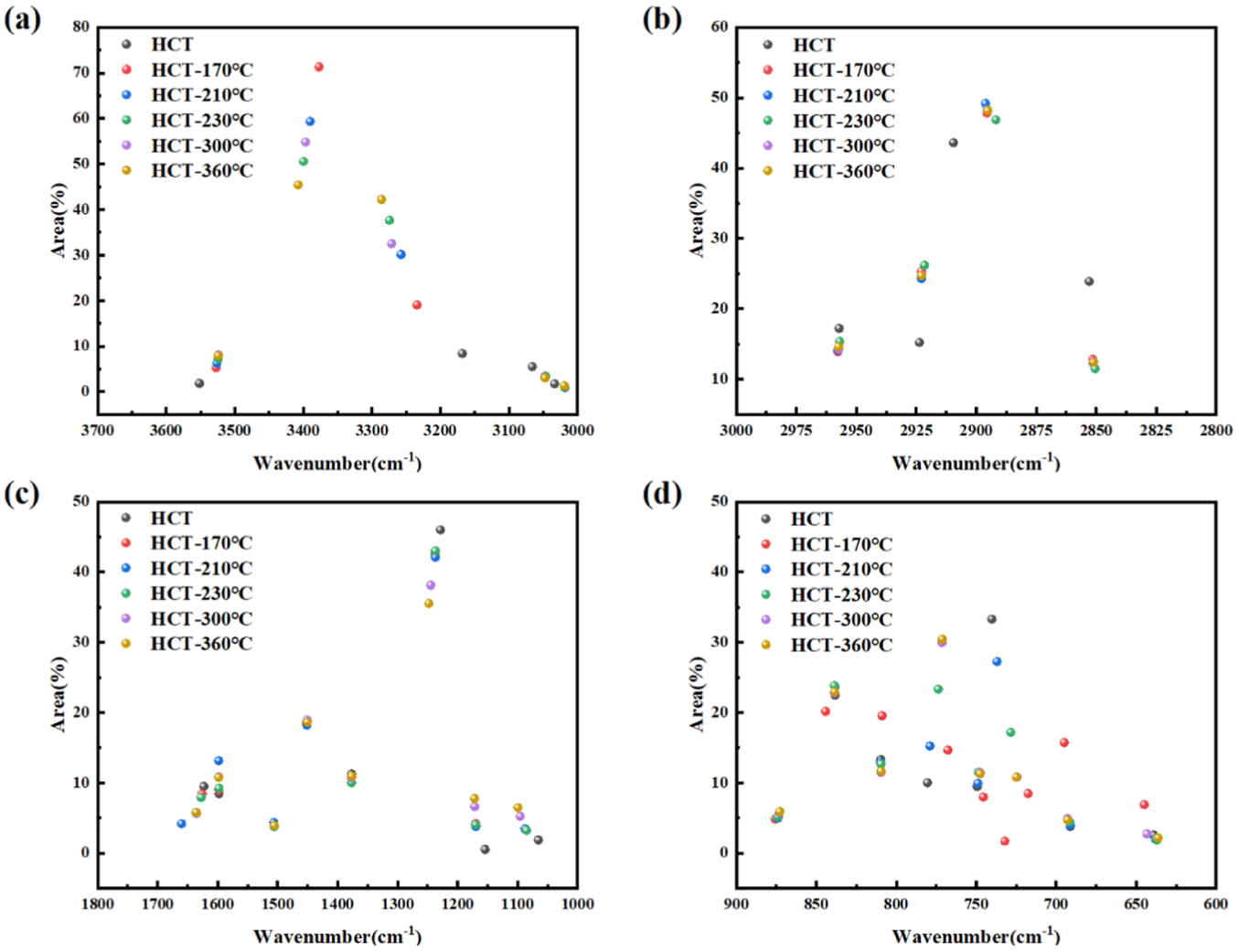

Figure 8. Distribution of fitting peaks of different fractions of HCT in different ranges. (a) Hydroxyl structure region, (b) fatty hydrocarbon structure region, (c) oxygen-containing functional group structure region, and (d) aromatic hydrocarbon structure region.

The infrared spectra of HCT cut by different fractions were analyzed using the PCA for Spectroscopy App in Origin software. The results are shown in Figure 9a. By considering the infrared spectrum of HCT as a reference, it was determined that when the number of main components was set to 2, the cumulative amount reached 96.93%. This indicates that there were two principal peaks in the infrared spectrum that could be used for analysis.[24] Based on this information, the peaks in PC1 and PC2 were identified and extracted. PC1 exhibited strong peak signals near 749 and 687 cm^{-1}. It displayed a general decrease in fitting peak intensity within the range of 750−700 cm^{-1}. PC2 showed strong peak signals near 2356 and 1143 cm^{-1}; it corresponded to the pattern of increasing fitting peak intensity as the distillation temperature increases within the range of 1200−1000 cm^{-1}. These observations suggest that the structure of aromatic hydrocarbon in HCTs varied significantly, and the presence of oxygen-containing functional groups had a certain influence on it.[25] In other regions, the influence was relatively minor. Furthermore, the samples HCT-210 °C, HCT-230 °C, HCT-300 °C, and HCT-360 °C in Figure 9b showed similar consistency. This similarity can be attributed to the distillation process, where, as the distillation temperature increased, lighter hydrocarbon products were separated from the raw materials, resulting in a decrease in the remaining oil product fraction. However, the specific composition and content of the remaining oil product varied among these samples. It can be clearly seen in the simulated distillation data, while the infrared spectrum cannot be obtained intuitively.

4. CONCLUSIONS

In this paper, the changes in the composition of heavy tar obtained from tar-rich coal through fractionation was studied. We analyzed the oil products using simulated distillation gas chromatography and conducted FTIR and PCA analyses on different fractions. The fraction content in the tar exhibited variations after simulated distillation at different temperatures. The light oil content decreased from 4.3 to 0.1%, and the asphalt content increased from 77.6 to 90.6%. This indicated that the production of light oil products decreases as the distillation temperature increases, while the content of heavy components would continue to increase. The fitted curves in the hydroxyl structure region, fatty hydrocarbon structure region, and oxygen-containing functional group structure region were relatively similar, while they were relatively different in the aromatic hydrocarbon structure region. It was mainly reflected in the distribution of fitted peaks and PCA. Compared to the peak of the reference spectrum, the

https://doi.org/10.1021/acsomega.3c07671
ACS Omega 2024, 9, 1352−1361

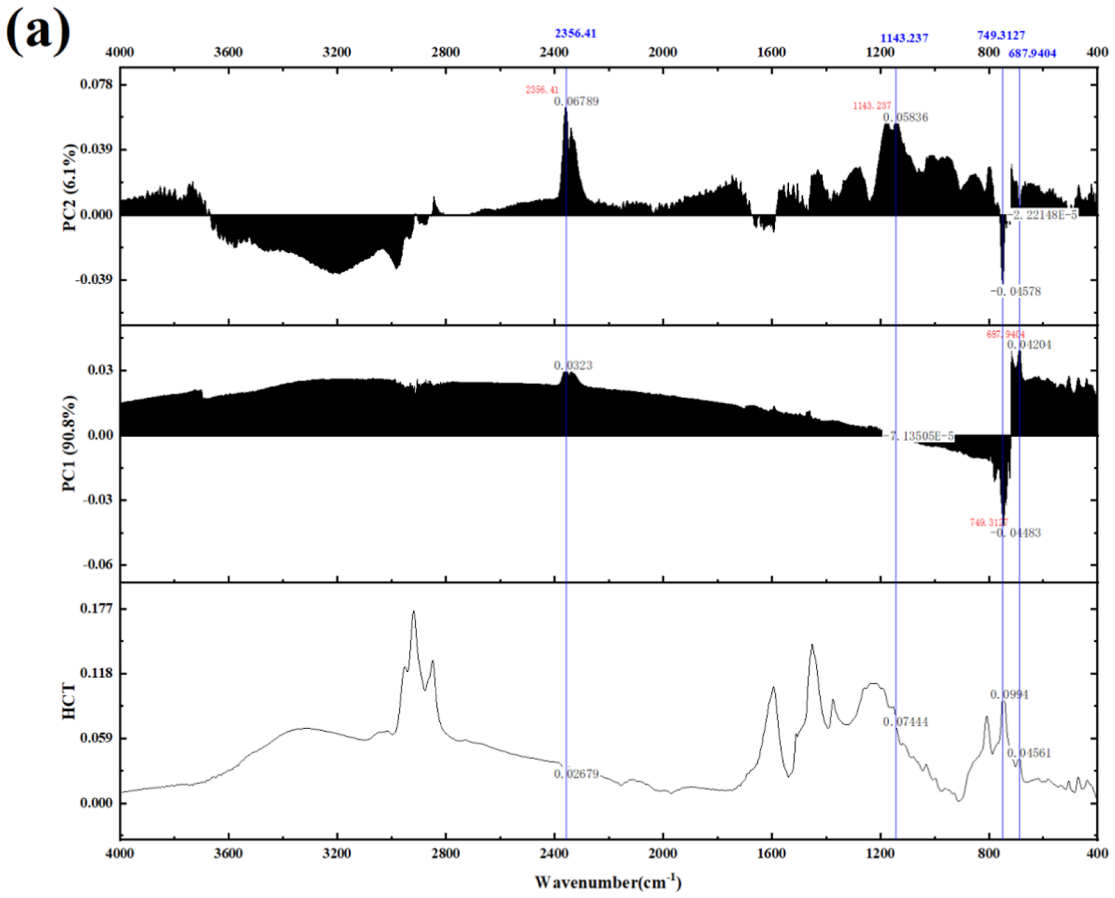

Figure 9. Loading with the reference spectrum plot and the score plot of PCA for spectroscopy: (a) T loading with the reference spectrum plot and (b) score plot.

https://doi.org/10.1021/acsomega.3c07671
ACS Omega 2024, 9, 1352−1361

difference of FTIR was mainly focused in 750−700 cm^{-1}, which was consistent with the previous conclusion.

AUTHOR INFORMATION

Corresponding Author

Hao Shu − *State Key Laboratory of Eco-hydraulics in Northwest Arid Region, Xi'an University of Technology, Xi'an 710048, China;* orcid.org/0000-0002-9757-1760; Email: 490258879@qq.com

Authors

Zhonghua Zhang − *Xi'an University of Science and Technology, Xi'an 710054, China*

Zhao Xue − *Xi'an University of Science and Technology, Xi'an 710054, China*

Complete contact information is available at: https://pubs.acs.org/10.1021/acsomega.3c07671

Author Contributions

Conceptualization: Z.X.; methodology: H.S.; software: Z.X.; validation: Z.X.; investigation: H.S.; data curation: S.H.; writing—original draft preparation: Z.X.; and writing—review and editing: Zhonghua Zhang.

Notes

The authors declare no competing financial interest.

ACKNOWLEDGMENTS

This research was funded by the Key Research and Development Program of Shaanxi (grant no. 2023-YBSF-282); Application Technology R&D and Achievement Transformation Plan of Beilin (grant no. GX2237); Shaanxi Province Postdoctoral Science Foundation (grant no. 2023BSHEDZZ252); Xianyang Key Research and Development Project (grant no. L2023-ZDYF-SF-009); and Open Fund of Shaanxi Key Laboratory of Geological Support for Coal Green Exploitation (grant no. DZBZ2020-08).

REFERENCES

(1) Li, A.; Zhu, C.; Zhang, L. Z.; Ma, Y. X.; Xu, D. M.; Gao, J.; Wang, Y. L. Efficient extraction and theoretical insights for separating o-, m-, and p-cresol from model coal tar by an ionic liquid Emim DCA. *Can. J. Chem. Eng.* **2022**, *100*, S205−S212.

(2) Pyshyev, S.; Demchuk, Y.; Poliuzhyn, I.; Kochubei, V. Obtaining and use adhesive promoters to bitumen from the phenolic fraction of coal tar. *Int. J. Adhes. Adhes.* **2022**, *118*, 103191.

(3) Li, L.; Lin, X. C.; Zhang, Y. K.; Dai, J. Z.; Xu, D. P.; Wang, Y. G. Characteristics of the mesophase and needle coke derived from the blended coal tar and biomass tar pitch. *J. Anal. Appl. Pyrol.* **2020**, *150*, 104889.

(4) Kalidindi, S.; Vinayak, S. A.; Biswas, S.; Kumaresan, D.; Prasad, R. K. Extraction of phenols from coal tar oil using binary solvents and ionic liquid mixture. *Int. J. Oil, Gas Coal Technol.* **2020**, *23* (2), 240−260.

(5) Ozbay, N.; Yargic, A. S. Carbon foam production from bio-based polyols of liquefied spruce tree sawdust: Effects of biomass/solvent mass ratio and pyrolytic oil addition. *J. Appl. Polym. Sci.* **2019**, *136* (11), 47185.

(6) Shi, J. L.; Ma, C. Preparation and characterization of spinnable mesophase pitches: A review. *New Carbon Mater.* **2019**, *34* (3), 211−219.

(7) Hata, Y.; Hayashizaki, H.; Takahashi, T.; Kanehashi, K. Structural Analysis of Primary Coal Tar by FD-MS. *ISIJ Int.* **2020**, *60* (9), 1892−1901.

(8) Hao, S.; Yuling, L.; Yang, J. Construction of Cu-BTC by carboxylic acid organic ligand and its application in low temperature SCR denitration. *Sci. Total Environ.* **2022**, *820*, 152984.

(9) Zhang, X.-Q.; Kang, Y.-H.; Gao, J.; Xiong, L.; Gao, Y.; Chen, T.; Liu, G.-H.; Wang, A.-M.; Wei, X.-Y.; Zong, Z.-M.; et al. Effective hydroconversion of heteroatom-containing organic species from the extraction of low-temperature coal tar to cycloalkanes over a Y/Beta composite zeolite supported nickel nanoparticles. *Fuel* **2022**, *321*, 124062.

(10) Avid, B.; Battsetseg, M.; Purevsuren, B.; Shiirav, G.; Kuznetsov, P. N.; Kuznetsova, L. I.; Kamenskii, E. S. Properties of pitch-like materials obtained using coal extraction. *Carbon Lett.* **2022**, *32* (2), 605−614.

(11) Lei, Z.; Liang, Q.; Ling, Q.; Cui, P.; Zhao, Z. Investigating the reaction mechanism of light tar for Shenfu bituminous coal pyrolysis. *Energy* **2023**, *263*, 125731.

(12) Xin, L.; Li, C.; Liu, W.; Xu, M.; Xie, J.; Han, L.; An, M. Change of sandstone microstructure and mineral transformation nearby UCG channel. *Fuel Process. Technol.* **2021**, *211*, 106575.

(13) Bhatta, R.; Dash, N.; Nayak, B. Effect of Heat on Organic and Inorganic Components in Some Non-coking Lower Gondwana Coals. *Trans. Indian Inst. Met.* **2021**, *74* (2), 387−397.

(14) Anto, R.; Bhui, U. K. Surfactant flooding for enhanced oil recovery-Insights on oil solubilization through optical spectroscopic approach. *J. Pet. Sci. Eng.* **2022**, *208*, 109803.

(15) Liu, Y.; Zhu, Y.; Mu, B.; Wang, Y.; Quan, Z.; Wang, A. Synthesis, characterization, and swelling behaviors of sodium carboxymethyl cellulose-g-poly(acrylic acid)/semi-coke superabsorbent. *Polym. Bull.* **2022**, *79* (2), 935−953.

(16) Chen, L.; Guo, F.; Wu, J.; Li, P.; Zhang, Y. Research on Coal Tar Pitch Catalytic Oxidation and Its Effect on the Emission of PAHs during Co-Carbonation with Coal. *Catalysts* **2021**, *11* (12), 1428.

(17) Wang, D.; Peng, Z.; Wang, J.; Liang, L.; Tu, C.; Zhang, Q.; Huang, W. Study on pyrolysis behavior of the coal fractions based on macro maceral separation. *Fuel* **2021**, *305*, 121572.

(18) Wu, Y.; Zhang, Y.; Zhuo, J.; Yao, Q. Effect of ion-exchangeable calcium on carbonaceous particulate matter formation during coal pyrolysis. *Fuel* **2022**, *315*, 123124.

(19) Shi, S.; Li, N.; Zhang, Y.; Ban, Y.; Song, Y.; He, R.; Zhou, H.; Liu, Q. Synergistic Catalytic Effect of Inherent Minerals and Specific Structures on the Steam Gasification of Lignite and Anthracite. *Int. J. Coal Prep. Util.* **2022**, *42* (2), 203−219.

(20) Sun, H.; Feng, D.; Sun, S.; Zhao, Y.; Zhang, L.; Chang, G.; Guo, Q.; Wu, J.; Qin, Y. Thermal evolution of gas-liquid-solid products and migration regulation of C/H/O elements during biomass pyrolysis. *J. Anal. Appl. Pyrol.* **2021**, *156*, 105128.

(21) Hao, S.; Yuling, L.; Yang, J.; Chuanchuan, D. Synthesis of Cu-Ce-BTC catalyst and its catalytic performance for denitration and synergistic mercury removal. *J. Environ. Chem. Eng.* **2023**, *11*, 109678.

(22) Zhang, C.-Y.; Wu, Q.; Wang, Y.-D.; Fan, J.-T.; Zhu, Z.-Z. Study on the Differences of Chemical Structures and Pyrolysis Characteristics between the Jurassic and Carboniferous Coking Coals. *ACS Omega* **2022**, *7* (8), 6768−6777.

(23) Hao, S.; Yuling, L.; Yang, J.; Chuanchuan, D.; Feng, B. Halogen modified Cu-Ce-BTC catalyst for NH3-SCR: Combination of NO and Hg0 removal experiments and mechanism analysis. *Sep. Purif. Technol.* **2023**, *327*, 124940.

(24) Yu, J.; Wang, C.; Wang, Y.; Qiu, L.; Yin, Y.; Li, X.; Zhao, F.; Chang, H. Poisoning Effects of HCl on MO_x-WO_3/TiO_2 (M=Mn, Ce and V) Catalysts for Selective Catalytic Reduction of NO_x by NH_3. *ChemCatChem* **2023**, *15*, 201093.

(25) Song, Q.; Zhao, H.-Y.; Ma, Q.-X.; Yang, L.; Ma, L.; Wu, Y.; Zhang, P. Catalytic upgrading of coal volatiles with Fe_2O_3 and hematite by TG-FTIR and Py-GC/MS. *Fuel* **2022**, *313*, 122667.